The Unified Discrete Surface Ricci flow

Min Zhang[a,*], Ren Guo[b], Wei Zeng[c], Feng Luo[d], Shing-Tung Yau[e], Xianfeng Gu[a]

[a]*Department of Computer Science, Stony Brook University, NY 11794, USA*
[b]*Department of Mathematics, Oregon State University, OR 97331, USA*
[c]*School of Computing and Information Sciences, Florida International University, FL 33199, USA*
[d]*Department of Mathematics,Rutgers University, NJ 08854, USA*
[e]*Deaprment of Mathematics,Harvard University, MA 02138, USA*

Abstract

Ricci flow deforms the Riemannian metric proportionally to the curvature, such that the curvature evolves according to a heat diffusion process and eventually becomes constant everywhere. Ricci flow has demonstrated its great potential by solving various problems in many fields, which can be hardly handled by alternative methods so far.

This work introduces the unified theoretic framework for discrete Surface Ricci Flow, including all the common schemes: Tangential Circle Packing, Thurston's Circle Packing, Inversive Distance Circle Packing and Discrete Yamabe Flow. Furthermore, this work also introduces a novel schemes, Virtual Radius Circle Packing and the Mixed Type schemes, under the unified framework. This work gives explicit geometric interpretation to the discrete Ricci energies for all the schemes with all back ground geometries, and the corresponding Hessian matrices.

The unified frame work deepens our understanding to the the discrete surface Ricci flow theory, and has inspired us to discover the new schemes, improved the flexibility and robustness of the algorithms, greatly simplified the implementation and improved the efficiency. Experimental results show the unified surface Ricci flow algorithms can handle general surfaces with different topologies, and is robust to meshes with different qualities, and is effective for solving real problems.

Keywords: Unified, Ricci flow, circle packing, discrete Ricci energy. Hessian matrix.

1. Introduction

Ricci flow was introduced by Hamilton for the purpose of studying low dimensional topology. Ricci flow deforms the Riemannian metric proportional to the curvature, such that the curvature evolves according to a heat diffusion process, and eventually becomes constant everywhere. In pure theory field, Ricci flow has been used for the proof of Poincaré's conjecture. In engineering fields, surface Ricci flow has been broadly applied for tackling many important problems, such as parameterization in graphics [1], deformable surface registration in vision [2], manifold spline construction in geometric modeling [3] and cancer detection in medical imaging [4]. More applications in engineering and medicine fields can be found in [5].

Suppose $(S, \mathbf{g})$ is a metric surface, according to the Gauss-Bonnet theorem, the total Gaussian curvature $\int_S K dA_{\mathbf{g}}$ equals to $2\pi\chi(S)$, where K is the Gaussian curvature, $\chi(S)$ the Euler characteristics of S. Ricci flow deforms the Riemannian metric conformally, namely, $\mathbf{g}(t) = e^{2u(t)}\mathbf{g}(0)$, where $u(t) : S \to \mathbb{R}$ is the conformal factor. The normalized Ricci flow can be written as

$$\frac{du(t)}{dt} = \frac{2\pi\chi(S)}{A(0)} - K(t). \quad (1.1)$$

where $A(0)$ is the initial surface area. Hamilton [6] and chow [7] proved the convergence of surface Ricci flow. Surface Ricci flow is the negative gradient flow of the Ricci energy. It is a powerful tool for designing Riemannian metrics using prescribed curvatures, which has great potential for many applications in engineering fields. Surface Ricci flow implies the celebrated surface uniformization theorem as shown in Fig.1. For surfaces with boundaries, uniformization theorem still holds as illustrated in Fig.2, where surfaces are conformally mapped to the circle domains on surfaces with

*Corresponding author
Email addresses:* mzhang@cs.sunysb.edu (Min Zhang), guore@math.oregonstate.edu (Ren Guo), wzeng@cs.fiu.edu (Wei Zeng), fluo@math.rutgers.edu (Feng Luo), yau@math.harvard.edu (Shing-Tung Yau), gu@cs.sunysb.edu (Xianfeng Gu)
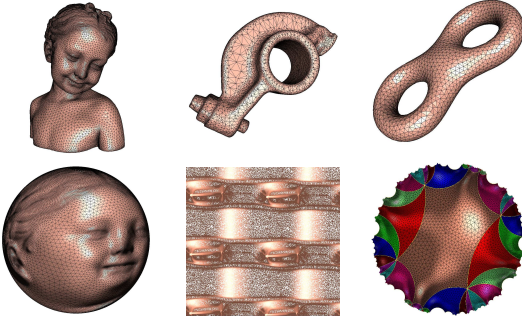
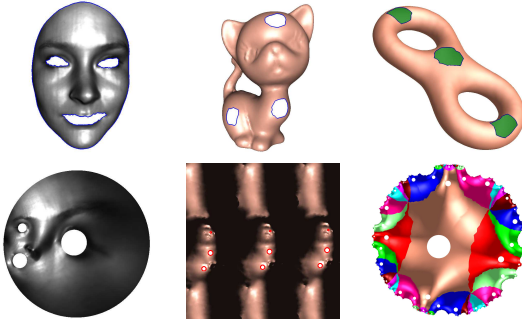Figure 1: Uniformization for closed surfaces by Ricci flow.

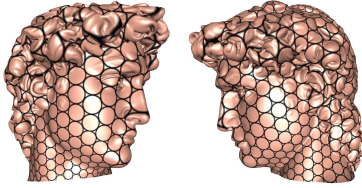Figure 2: Uniformization for surfaces with boundaries by Ricci flow.

Figure 3: Conformal mapping preserves infinitesimal circles.

constant curvatures.

Conformal metric deformation transforms infinitesimal circles to infinitesimal circles as shown in Fig. 3. Intuitively, one approximates the surface by a triangulated polyhedron (a triangle mesh), covers each vertex by a disk of finite size (a cone), and deforms the disk radii preserving the combinatorial structure of the triangulation and the intersection angles among the circles. This deformation simulates the smooth conformal mapping with very high fidelity. Rodin and Sullivan [8] proved that if the triangulation of a simply connected planar domain is subdivided infinite times, the induced discrete conformal mappings converge to the smooth Riemann mapping. The discrete version of surface Ricci flow was introduced by Chow and Luo in [9] in 2003. It is based on the circle packing method.

Historically, many schemes of circle packing or circle pattern have been invented. The discrete surface can be constructed by gluing Spherical, Euclidean or Hyperbolic triangles isometrically along their edges. Accordingly, we say the triangle mesh has spherical $\mathbb{S}^2$, Euclidean $\mathbb{E}^2$ or hyperbolic $\mathbb{H}^2$ background geometry. Under each background geometry, there are 6 schemes, tangential circle packing, Thurston's circle packing, inversive distance circle packing, discrete Yamabe flow, virtual radius circle packing and mixed type scheme. There are 18 combinations in total. Among them, the hyperbolic and spherical virtual radius circle packing and mixed type schemes are first introduced in this work.

Most of the existing schemes were invented and developed individually in the past. This work seeks a coherent theoretic framework, which can unify all the existing schemes, and predicts undiscovered ones. This leads to deeper understandings of discrete surface Ricci flow and provides approaches for further generalization. In practice, the theoretic discovery of virtual radius circle packing gives novel computational algorithm; the mixed schemes improves the flexibility; the unified framework greatly simplifies the implementation; the geometric interpretations offer better intuitions.

1.1. Contributions

This work has the following contributions:

1. This work establishes a unified framework for discrete surface Ricci flow, which covers most existing schemes: tangential circle packing, Thurston's circle packing, inversive distance circle packing, discrete Yamabe flow, virtual radius circle packing and mixed type schemes, in Spherical, Euclidean and hyperbolic background geometry. In Euclidean case, our unified framework is equivalent to Glickenstein's geometric formulation [10].To the best of our knowledge, the unified frameworks for both hyperbolic and spherical schemes are reported for the first time.

2. This work introduces 4 novel schemes for discrete surface Ricci flow: virtual radius circle packing and mixed type schemes under both hyperbolic and Euclidean background geometries, which are naturally deduced from our unification work. To the best of our knowledge, these are introduced to the literature for the first time.

3. This work gives an explicit geometric interpretation to the discrete Ricci energy for all the 18 schemes. The geometric interpretations to 2 Yamabe flow schemes (both Euclidean and Hyperbolic)

2

were first made by Bobenko, Pinkall and Springborn [11].

4. This work also provides an explicit geometric interpretation to the Hessian of discrete Ricci energy for all the 18 schemes. The interpretation in Euclidean case is due to Glickenstein [10]. To the best of our knowledge, the interpretation in Hyperbolic and Spherical cases are introduced for the first time. Recently, Glickenstein and Thomas discovered the similar result independently [12].

The paper is organized as follows: section 2 briefly reviews the most related theoretic works; section 3 introduces the unified framework for different schemes of discrete surface Ricci flow, which covers 18 schemes in total; section 4 explains the geometric interpretation of the Hessian matrix of discrete Ricci energy for all schemes with different background geometries; section 5 gives a geometric interpretation of Ricci energy; Experimental results are reported in section 6, different schemes are systematically compared. The work concludes in section 7, future directions are discussed; Finally, in the appendix, we give the implementation details and reorganize all the formulae.

2. Previous Works

Thurston's Circle Packing. In his work on constructing hyperbolic metrics on 3-manifolds, Thurston [13] studied a Euclidean (or a hyperbolic) circle packing on a triangulated closed surface with prescribed intersection angles. His work generalizes Koebe's and Andreev's results of circle packing on a sphere [14, 15, 16]. Thurston conjectured that the discrete conformal mapping based on circle packing converges to the smooth Riemann mapping when the discrete tessellation becomes finer and finer. Thurston's conjecture has been proved by Rodin and Sullivan [8]. Chow and Luo established the intrinsic connection between circle packing and surface Ricci flow [9].

The rigidity for classical circle packing was proved by Thurston [13], Marden-Rodin [17], Colin de Verdiére [18], Chow-Luo [9], Stephenson [19], and He [20].

Inversive Distance Circle Packing. Bowers-Stephenson [21] introduced inversive distance circle packing which generalizes Andreev-Thurston's intersection angle circle packing. See Stephenson [19] for more information. Guo gave a proof for local rigidity [22] of inversive distance circle packing. Luo gave a proof for global rigidity in [23].

Yamabe Flow. Luo introduced and studied the combinatorial Yamabe problem for piecewise flat metrics on triangulated surfaces [24]. Springborn, Schröder and Pinkall [25] considered this combinatorial conformal change of piecewise flat metrics and found an explicit formula of the energy function. Glickenstein [26, 27] studied the combinatorial Yamabe flow on 3-dimensional piecewise flat manifolds. Bobenko-Pinkall-Springborn introduced a geometric interpretation to Euclidean and hyperbolic Yamabe flow using the volume of generalized hyperbolic tetrahedron in [11]. Combinatorial Yamabe flow on hyperbolic surfaces with boundary has been studied by Guo in [28]. The existence of the solution to Yamabe flow with topological surgeries has been proved recently in [29] and [30].

Virtual Radius Circle Packing. The Euclidean virtual radius circle packing first appeared in [5]. The hyperbolic and spherical virtual radius circle packing are introduced in this work.

Mixed type Circle Packing. The Euclidean mixed type circle packing appeared in [5] and Glickenstein's talk [31]. This work introduces hyperbolic and spherical mixted type schemes.

Unified Framework. Recently Glickenstein [10] set the theory of combinatorial Yamabe flow of piecewise flat metric in a broader context including the theory of circle packing on surfaces. This work focuses on the hyperbolic and spherical unified frameworks.

Variational Principle. The variational approach to circle packing was first introduced by Colin de Verdiére [18]. Since then, many works on variational principles on circle packing or circle pattern have appeared. For example, see Brägger [32], Rivin [33], Leibon [34], Chow-Luo [9], Bobenko-Springborn [35], Guo-Luo [36], and Springborn [37]. Variational principles for polyhedral surfaces including the topic of circle packing were studied systematically in Luo [38]. Many energy functions are derived from the cosine law and its derivative. Tangent circle packing is generalized to tangent circle packing with a family of discrete curvature. For exposition of this work, see also Luo-Gu-Dai [39].

Discrete Uniformization. Recently, Gu et al established discrete uniformization theorem based on Euclidean [29] and hyperbolic [30] Yamabe flow. In a series of papers on developing discrete uniformization theorem [40],[41],[42] and [43], Sa'ar Hersonsky proved several important theorems based on discrete harmonic maps and cellular decompositions. His approach is complementary to the work mentioned above.
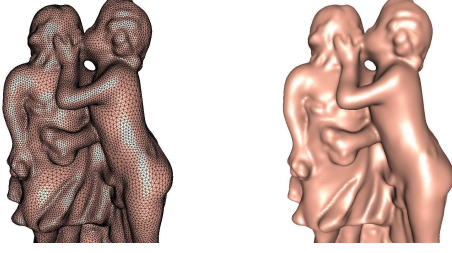
Figure 4: Smooth surfaces are approximated by discrete Surfaces

3. Unified Discrete Surface Ricci Flow

This section systematically introduces the unified framework for discrete surface Ricci flow. The whole theory is explained using the variational principle on discrete surfaces based on derivative cosine law [39]. The elementary concepts and some of schemes can be found in [38] and the chapter 4 in [5].

3.1. Elementary Concepts

In practice, smooth surfaces are usually approximated by *discrete surfaces*. Discrete surfaces are represented as two dimensional simplicial complexes which are manifolds, as shown in Fig. 4.

Definition 3.1 (Triangular Mesh). *Suppose Σ is a two dimensional simplicial complex, furthermore it is also a manifold, namely, for each point p of Σ, there exists a neighborhood of p, $U(p)$, which is homeomorphic to the whole plane or the upper half plane. Then Σ is called a triangular mesh.*

If $U(p)$ is homeomorphic to the whole plane, then p is called an interior point; if $U(p)$ is homeomorphic to the upper half plane, then p is called a boundary point.

The fundamental concepts from smooth differential geometry, such as Riemannian metric, curvature and conformal structure, are generalized to the simplicial complex, respectively.

In the following discussion, we use $\Sigma = (V, E, F)$ to denote the mesh with vertex set V, edge set E and face set F. A discrete surface is with Euclidean (hyperbolic or spherical) background geometry if it is constructed by isometrically gluing triangles in $\mathbb{E}^2$ ($\mathbb{H}^2$ or $\mathbb{S}^2$).

Definition 3.2 (Discrete Riemannian Metric). *A discrete metric on a triangular mesh is a function defined on the edges, $l : E \to \mathbb{R}^+$, which satisfies the triangle inequality: on each face $[v_i, v_j, v_k]$, l_i, l_j, l_k are the lengths of edges against v_i, v_j, v_k respectively,*

$$l_i + l_j > l_k, \ l_j + l_k > l_i, \ l_k + l_i > l_j.$$

A triangular mesh with a discrete Riemannian metric is called a discrete metric surface.
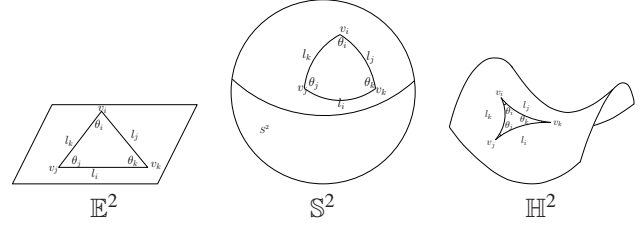

Figure 5: Different background geometry, Euclidean, spherical and hyperbolic.

Definition 3.3 (Background Geometry). *Suppose Σ is a discrete metric surface, if each face of Σ is a spherical, (Euclidean or hyperbolic) triangle, then we say Σ is with spherical, (Euclidean or hyperbolic) background geometry. We use $\mathbb{S}^2$, $\mathbb{E}^2$ and $\mathbb{H}^2$ to represent spherical Euclidean or hyperbolic background metric.*

Triangles with different background geometries satisify different cosine laws:

$$
\begin{aligned}
1 &= \frac{\cos\theta_i + \cos\theta_j \cos\theta_k}{\sin\theta_j \sin\theta_k} & \mathbb{E}^2 \\
\cos l_i &= \frac{\cos\theta_i + \cos\theta_j \cos\theta_k}{\sin\theta_j \sin\theta_k} & \mathbb{S}^2 \\
\cosh l_i &= \frac{\cosh\theta_i + \cosh\theta_j \cosh\theta_k}{\sinh\theta_j \sinh\theta_k} & \mathbb{H}^2
\end{aligned}
$$

The discrete Gaussian curvature is defined as angle deficit, as shown in Fig. 6.

Definition 3.4 (Discrete Gauss Curvature). *The discrete Gauss curvature function on a mesh is defined on vertices, $K : V \to \mathbb{R}$,*

$$K(v) = \begin{cases} 2\pi - \sum_{jk} \theta_i^{jk}, & v \notin \partial M \\ \pi - \sum_{jk} \theta_i^{jk}, & v \in \partial M \end{cases},$$

where θ_i^{jk}'s are corner angle at v_i in the face $[v_i, v_j, v_k]$, and ∂M represents the boundary of the mesh.
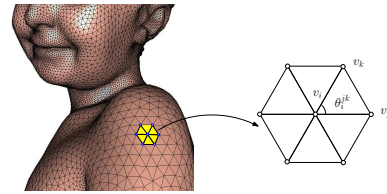

Figure 6: Discrete curvatures of an interior vertex

The Gauss-Bonnet theorem still holds in the discrete case.

4

Theorem 3.5 (Discrete Gauss-Bonnet Theorem).
Suppose Σ is a triangular mesh with Euclidean background metric. The total curvature is a topological invariant,

$$\sum_{v \notin \partial \Sigma} K(v) + \sum_{v \in \partial \Sigma} K(v) + \varepsilon A(\Sigma) = 2\pi \chi(\Sigma), \quad (3.1)$$

where χ is the characteristic Euler number, and K is the Gauss curvature, $A(\Sigma)$ is the total area, $\varepsilon = \{+1, 0, -1\}$ if Σ is with spherical, Euclidean or hyperbolic background geometry.

3.2. Unified Circle Packing Metrics

Definition 3.6 (Circle Packing Metric). *Suppose $\Sigma = (V, E, F)$ is a triangle mesh with spherical, Euclidean or hyperbolic background geometry. Each vertex v_i is associated with a circle with radius γ_i. The circle radius function is denoted as $\gamma : V \to \mathbb{R}_{>0}$; a function defined on the vertices $\varepsilon : V \to \{+1, 0, -1\}$ is called the scheme coefficient; a function defined on edges $\eta : E \to \mathbb{R}$ is called the discrete conformal structure coefficient. A circle packing metric is a 4-tuple $(\Sigma, \gamma, \eta, \varepsilon)$, the edge length is determined by the 4-tuple and the background geometry.*

In the smooth case, changing a Riemannian metric by a scalar function, $\mathbf{g} \to e^{2u} \mathbf{g}$, is called a conformal metric deformation. The discrete analogy to this is as follows.

Definition 3.7 (Discrete Conformal Equivalence).
Two circle packing metrics $(\Sigma_k, \gamma_k, \eta_k, \varepsilon_k)$, $k = 1, 2$, are conformally equivalent if $\Sigma_1 = \Sigma_2$, $\eta_1 = \eta_2$, $\varepsilon_1 = \varepsilon_2$. ($\gamma_1$ may not equals to γ_2.)

The discrete analogy to the concept of conformal factor in the smooth case is

Definition 3.8 (Discrete Conformal Factor). *Discrete conformal factor for a circle packing metric $(\Sigma, \gamma, \eta, \varepsilon)$ is a function defined on each vertex $\mathbf{u} : V \to \mathbb{R}$,*

$$u_i = \begin{cases} \log \gamma_i & \mathbb{E}^2 \\ \log \tanh \frac{\gamma_i}{2} & \mathbb{H}^2 \\ \log \tan \frac{\gamma_i}{2} & \mathbb{S}^2 \end{cases} \quad (3.2)$$

Definition 3.9 (Circle Packing Schemes). *Suppose $\Sigma = (V, E, F)$ is triangle mesh with spherical, Euclidean or hyperbolic background geometry. Given a circle packing metric $(\Sigma, \gamma, \eta, \varepsilon)$, for an edge $[v_i, v_j] \in E$, its*

(a) tangential CP   (b) Thurston's CP   (c) Inversive distance CP

$\eta = 1, \varepsilon = 1$ $0 \le \eta \le 1, \varepsilon = 1$ $\eta \ge 1, \varepsilon = 1$
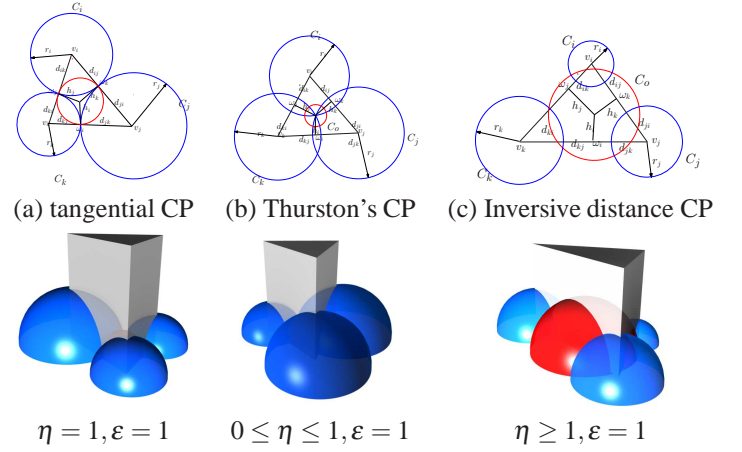
Figure 7: Tangential circle packing, Thurston's circle packing and inversive distance circle packing schemes, and the geometric interpretations to their Ricci energies.
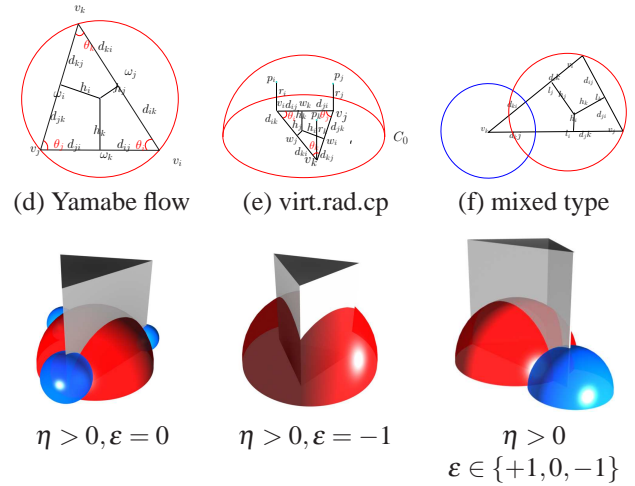

(d) Yamabe flow   (e) virt.rad.cp   (f) mixed type

$\eta > 0, \varepsilon = 0$ $\eta > 0, \varepsilon = -1$ $\eta > 0$
$\varepsilon \in \{+1, 0, -1\}$

Figure 8: Yamabe flow, virtual radius circle packing and mixed type schemes, and the geometric interpretations to their Ricci energies.

length l_{ij} is given by

$$\begin{cases} l_{ij}^2 = 2\eta_{ij} e^{u_i + u_j} + \varepsilon_i e^{2u_i} + \varepsilon_j e^{2u_j} & \mathbb{E}^2 \\ \cosh l_{ij} = \dfrac{4\eta_{ij} e^{u_i + u_j} + (1 + \varepsilon_i e^{2u_i})(1 + \varepsilon_j e^{2u_j})}{(1 - \varepsilon_i e^{2u_i})(1 - \varepsilon_j e^{2u_j})} & \mathbb{H}^2 \\ \cos l_{ij} = \dfrac{-4\eta_{ij} e^{u_i + u_j} + (1 - \varepsilon_i e^{2u_i})(1 - \varepsilon_j e^{2u_j})}{(1 + \varepsilon_i e^{2u_i})(1 + \varepsilon_j e^{2u_j})} & \mathbb{S}^2 \end{cases} \quad (3.3)$$

The schemes are named as follows:

Scheme	ε_i	ε_j	η_{ij}
Tangential Circle Packing	+1	+1	+1
Thurston's Circle Packing	+1	+1	[0,1]
Inversive Distance Circle Packing	+1	+1	> 0
Yamabe Flow	0	0	> 0
Virtual Radius Circle Packing	-1	-1	> 0
Mixed type	{−1,0,+1}	{−1,0,+1}	> 0

5

Fig. 7 and Fig. 8 illustrate all the schemes with for discrete surfaces with Euclidean background geometry.

Remark 3.10. *From the definition, the tangential circle packing is a special case of Thurston's circle packing; Thurston's circle packing is a special case of inversive distance circle packing. In the following discussion, we unify all three types as inversive distance circle packing.*

3.3. Discrete Surface Ricci Flow

Definition 3.11 (Discrete Surface Ricci Flow). *A discrete surface with $\mathbb{S}^2$, $\mathbb{E}^2$ or $\mathbb{H}^2$ background geometry, and a circle packing metric $(\Sigma, \gamma, \eta, \varepsilon)$, the discrete surface Ricci flow is*

$$\frac{du_i(t)}{dt} = \bar{K}_i - K_i(t), \qquad (3.4)$$

where $\bar{K}_i$ is the target curvature at the vertex v_i.

The target curvature must satisfy certain constraints to ensure the existence of the solution to the flow, such as Gauss-Bonnet equation Eqn. 3.1, but also some additional ones described in [13], [17] and [9], for instances.

The discrete surface Ricci flow has exactly the same formula as the smooth counter part Eqn. 1.1. Furthermore, similar to the smooth case, discrete surface Ricci flow is also variational: the discrete Ricci flow is the negative gradient flow of the discrete Ricci energy.

Definition 3.12 (Discrete Ricci Energy). *A discrete surface with $\mathbb{S}^2$, $\mathbb{E}^2$ or $\mathbb{H}^2$ background geometry, and a circle packing metric $(\Sigma, \gamma, \eta, \varepsilon)$. For a triangle $[v_i, v_j, v_k]$ with inner angles $(\theta_i, \theta_j, \theta_k)$, the discrete Ricci energy on the face is given by*

$$E_f(u_i, u_j, u_k) = \int^{(u_i, u_j, u_k)} \theta_i du_i + \theta_j du_j + \theta_k du_k. \quad (3.5)$$

The discrete Ricci energy for the whole mesh is defined as

$$E_\Sigma(u_1, u_2, \cdots, u_n) = \int^{(u_1, u_2, \cdots, u_n)} \sum_{i=1}^{n} (\bar{K}_i - K_i) du_i.. \quad (3.6)$$

From definition, we get the relation between the surface Ricci energy and the face Ricci energy

$$E_\Sigma = \sum_{i=1}^{n} (\bar{K}_i - 2\pi) u_i + \sum_{f \in F} E_f. \qquad (3.7)$$

The description of the energy in terms of an integral requires the fact that the inside is a closed form so that it

is defined independent of the integration path. This follows from the following symmetry lemma, which has fundamental importance. In this work, we give three proofs. The following one is algebraic, more difficult to verify, but leads to computational algorithm directly. The second one is based on the geometric interpretation to the Hessian matrix in Section 4. The third one is based on the geometric interpretation to the discrete Ricci energy. The later two proofs are more geometric and intuitive.

Lemma 3.13 (Symmetry). *A discrete surface with $\mathbb{S}^2$, $\mathbb{E}^2$ or $\mathbb{H}^2$ background geometry, and a circle packing metric $(\Sigma, \gamma, \eta, \varepsilon)$, then for any pair of vertices v_i and v_j:*

$$\frac{\partial K_i}{\partial u_j} = \frac{\partial K_j}{\partial u_i}. \qquad (3.8)$$

Proof 3.14. *From the relation in Eqn. 3.7, it is sufficient and necessary to show the symmetry for each triangle $[v_i, v_j, v_k]$ for all schemes,*

$$\frac{\partial \theta_i}{\partial u_j} = \frac{\partial \theta_j}{\partial u_i}.$$

This is proven by finding the explicit formula for the Hessain matrix of the face Ricci energy,

$$\frac{\partial(\theta_i, \theta_j, \theta_k)}{\partial(u_i, u_j, u_k)} = -\frac{1}{2A} L\Theta L^{-1} D, \qquad (3.9)$$

where

$$A = \frac{1}{2} \sin \theta_i s(l_j) s(l_k) \qquad (3.10)$$

the matrix L

$$L = \begin{pmatrix} s(l_i) & 0 & 0 \\ 0 & s(l_j) & 0 \\ 0 & 0 & s(l_k) \end{pmatrix} \qquad (3.11)$$

and the matrix Θ

$$\Theta = \begin{pmatrix} -1 & \cos\theta_k & \cos\theta_j \\ \cos\theta_k & -1 & \cos\theta_i \\ \cos\theta_j & \cos\theta_i & -1 \end{pmatrix} \qquad (3.12)$$

and

$$D = \begin{pmatrix} 0 & \tau(i,j,k) & \tau(i,k,j) \\ \tau(j,i,k) & 0 & \tau(j,k,i) \\ \tau(k,i,j) & \tau(k,j,i) & 0 \end{pmatrix} \qquad (3.13)$$

where $s(x)$ and $\tau(i,j,k)$ are defined as

6

	$s(x)$	$\tau(i,j,k)$
$\mathbb{E}^2$	x	$1/2(l_i^2 + \varepsilon_j r_j^2 - \varepsilon_k r_k^2)$
$\mathbb{H}^2$	$\sinh x$	$\cosh l_i \cosh^{\varepsilon_j} r_j - \cosh^{\varepsilon_k} r_k$
$\mathbb{S}^2$	$\sin x$	$\cos l_i \cos^{\varepsilon_j} r_j - \cos^{\varepsilon_k} r_k$

By symbolic computation, it is straightforward to verify the symmetry of Eqn. 3.9.

4. Geometric interpretation to Hessian

This section focuses on the geometric interpretation to Hessian matrix of the discrete Ricci energy on each face for $\mathbb{E}^2, \mathbb{H}^2$ and $\mathbb{S}^2$ cases. This gives the second proof of the symmetry lemma 3.13.

4.1. Euclidean Case

The interpretation in Euclidean case is due to Glickenstein [10] (Z. He [44] in the case of circle packings) and illustrated in [5]. In the current work, we build the connection to the Power Delaunay triangulation and power voronoi diagram.

We only focus on one triangle $[v_i, v_j, v_k]$, with corner angles $\theta_i, \theta_j, \theta_k$, conformal factors u_i, u_j, u_k and edge lengths l_{ij} for edge $[v_i, v_j]$, l_{jk} for $[v_j, v_k]$ and l_{ki} for $[v_k, v_i]$.

Power Delaunay Triangulation. As shown in Fig. 7 and Fig. 8, the *power* of q with respect to v_i is

$$pow(v_i, q) = |v_i - q|^2 - \varepsilon \gamma_i^2.$$

The *power center o* of the triangle satisifies

$$pow(v_i, o) = pow(v_j, o) = pow(v_k, o).$$

The *power circle C* centered at o with radius γ, where $\gamma = pow(v_i, o)$.

Therefore, for tangential, Thurton's and inversive distance circle packing cases, the power circle is orthogonal to three circles at the vertices C_i, C_j and C_k; for Yamabe flow case, the power circle is the circumcircle of the triangle; for virtual radius circle packing, the power circle is the equator of the sphere, which goes through three points $\{v_i + \gamma_i^2 \mathbf{n}, v_j + \gamma_j^2 \mathbf{n}, v_k + \gamma_k^2 \mathbf{n}\}$, where $\mathbf{n}$ is the normal to the plane.

Through the power center, we draw line perpendicular to three edges, the perpendicular feets are w_i, w_j and w_k respectively. The distance from the power center to the perpendicular feet are h_i, h_j and h_k respectively. Then it can be shown easily that

$$\frac{\partial \theta_i}{\partial u_j} = \frac{\partial \theta_j}{\partial u_i} = \frac{h_k}{l_k}, \frac{\partial \theta_j}{\partial u_k} = \frac{\partial \theta_k}{\partial u_j} = \frac{h_i}{l_i}, \frac{\partial \theta_k}{\partial u_i} = \frac{\partial \theta_i}{\partial u_k} = \frac{h_j}{l_j}, \tag{4.1}$$

furthermore,

$$\frac{\partial \theta_i}{\partial u_i} = -\frac{h_k}{l_k} - \frac{h_j}{l_j}, \frac{\partial \theta_j}{\partial u_j} = -\frac{h_k}{l_k} - \frac{h_i}{l_i}, \frac{\partial \theta_k}{\partial u_k} = -\frac{h_i}{l_i} - \frac{h_j}{l_j}. \tag{4.2}$$

These two formula induces the formula for the Hessian of the Ricci energy of the whole surface. One can treat the circle packing $(\Sigma, \gamma, \eta, \varepsilon)$ as a power triangulation, which has a dual power diagram $\bar{\Sigma}$. Each edge $e_{ij} \in \Sigma$ has a dual edge $\bar{e} \in \bar{\Sigma}$, then

$$\frac{\partial K_i}{\partial u_j} = \frac{\partial K_j}{\partial u_i} = \frac{|\bar{e}_{ij}|}{|e_{ij}|}, \tag{4.3}$$

and

$$\frac{\partial K_i}{\partial u_i} = -\sum_j \frac{\partial K_i}{\partial u_j}. \tag{4.4}$$

This gives a geometric proof for the symmetry lemma 3.13 in Euclidean case.

Suppose on the edge $[v_i, v_j]$, the distance from v_i to the perpendicular foot w_k is d_{ij}, the distance from v_j to w_k is d_{ji}, then $l_{ij} = d_{ij} + d_{ji}$, and

$$\frac{\partial l_{ij}}{\partial u_i} = d_{ij}, \frac{\partial l_{ij}}{\partial u_j} = d_{ji},$$

furthermore

$$d_{ij}^2 + d_{jk}^2 + d_{ki}^2 = d_{ik}^2 + d_{kj}^2 + d_{ji}^2.$$

This shows the power circle interpretation is equivalent to Glikenstain's formulation.

4.2. Hyperbolic Case

Let $\triangle_{123}$ be a hyperbolic triangle whose vertices are labeled by $1, 2, 3$. Let r_1, r_2, r_3 be three positive numbers associated to the vertices, and $\varepsilon_1, \varepsilon_2, \varepsilon_3 \in \{-1, 0, 1\}$ be indicators of the type of the vertices.

For the mixed type of discrete conformal geometry, the edge length of $\triangle_{123}$ is given by

$$\cosh l_k = 4\eta_{ij} \frac{\sinh r_i}{(1-\varepsilon_i)\cosh r_i + 1 + \varepsilon_i} \frac{\sinh r_j}{(1-\varepsilon_j)\cosh r_j + 1 + \varepsilon_j} + \cosh^{\varepsilon_i} r_i \cosh^{\varepsilon_j} r_j,$$

where $\{i, j, k\} = 1, 2, 3$.

Via the cosine law, the edge lengths l_1, l_2, l_3 determine the angles $\theta_1, \theta_2, \theta_3$.

When $\varepsilon_1 = \varepsilon_2 = \varepsilon_3 = 0$, this is the case of Yamabe flow. There is a circle passing through the three vertices of $\triangle_{123}$. It is still called the *power circle*.

When $\varepsilon_1 = \varepsilon_2 = \varepsilon_3 = 1$, this is the case of inversive distance circle packing. Centered at each vertex i, there is a circle with radius r_i. Then there is the *power circle* orthogonal to the three circles centered at the vertices.

7

When $\varepsilon_1 = \varepsilon_2 = \varepsilon_3 = -1$, this is the case of virtual radius circle packing. Let $\triangle_{123}$ be on the equator plane of the ball model of the hyperbolic space $\mathbb{H}^3$. For each vertex i, let ii' be the geodesic arc perpendicular to the equator plane with length r_i. Assume $1', 2', 3'$ are above the equator plane. There is a hemisphere passing through $1', 2', 3'$ and orthogonal to the equator plane. The *power circle* in this case is the intersection of the hemisphere and the equator plane.

For a mix type, the power circle can still be defined.

For any type, let h_i be the distance from the center of the power circle to the edge ij whose length is l_k.

Theorem 4.1. *Let*

$$e^{u_i} = \frac{e^{r_i} - 1}{e^{r_i} + 1} = \tanh \frac{r_i}{2}.$$

Then

$$\frac{\partial \theta_1}{\partial u_2} = \frac{\partial \theta_2}{\partial u_1}$$

which equal to

$$\frac{\tanh h_3}{\sinh^2 l_3} \sqrt{2 \cosh^{\varepsilon_1} r_1 \cosh^{\varepsilon_2} r_2 \cosh l_3 - \cosh^{2\varepsilon_1} r_1 - \cosh^{2\varepsilon_2} r_2}.$$

This gives a geometric proof for the symmetry lemma 3.13 in hyperbolic case.

We only need to prove the theorem for the case of $\varepsilon_1 = \varepsilon_2 = \varepsilon_3 = 1$. General case can be proved similarly.

Proof 4.2. *Step 1.* *Denote the center of the power circle by o, the radius by r. Let x, y, z be the distance from o to the vertices $1, 2, 3$. Then*

$$\begin{aligned} \cosh x &= \cosh r \cosh r_1 \\ \cosh y &= \cosh r \cosh r_2 \quad (4.5) \\ \cosh z &= \cosh r \cosh r_3 \end{aligned}$$

Let α be the angle $\angle 13o$ and β the angle $\angle 23o$. Then $\alpha + \beta = \theta_3$. Therefore

$$1 + 2 \cos \alpha \cos \beta \cos \theta_3 = \cos^2 \alpha + \cos^2 \beta + \cos^2 \theta_3. \quad (4.6)$$

By the cosine law,

$$\cos \alpha = \frac{-\cosh x + \cosh z \cosh l_2}{\sinh z \sinh l_2},$$

$$\cos \beta = \frac{-\cosh y + \cosh z \cosh l_1}{\sinh z \sinh l_1},$$

$$\cos \theta_3 = \frac{-\cosh l_3 + \cosh l_1 \cosh l_2}{\sinh l_1 \sinh l_2}.$$

Substituting the three formulas into the equation (4.6), we obtain a relation between the 6 numbers l_1, l_2, l_3, x, y, z.

Substituting the equations (4.5) into this relation, we obtain a relation between $l_1, l_2, l_3, r_1, r_2, r_3$ and r.

Solving for r, we get $\cosh^2 r = \frac{\mathcal{N}}{\mathcal{D}}$, where

$$\mathcal{N} = 1 + 2 \cosh l_1 \cosh l_2 \cosh l_3 - \cosh^2 l_1 - \cosh^2 l_2 - \cosh^2 l_3,$$

$$\begin{aligned} \mathcal{D} &= \cosh^2 r_1 (1 - \cosh^2 l_1) + 2 \cosh r_2 \cosh r_3 (\cosh l_2 \cosh l_3 - \cosh l_1) \\ &\quad + \cosh^2 r_2 (1 - \cosh^2 l_2) + 2 \cosh r_3 \cosh r_1 (\cosh l_3 \cosh l_1 - \cosh l_2) \\ &\quad + \cosh^2 r_3 (1 - \cosh^2 l_3) + 2 \cosh r_1 \cosh r_2 (\cosh l_1 \cosh l_2 - \cosh l_3). \end{aligned}$$

Step 2. *Since h_3 is the height of the triangle $\triangle_{o12}$ with bottom the edge 12. By the standard formula of height of a hyperbolic triangle, we have*

$$\sinh^2 h_3 = \frac{1 + 2 \cosh x \cosh y \cosh l_3 - \cosh^2 x - \cosh^2 y - \cosh^2 l_3}{\sinh^2 l_3}.$$

After substituting the equations (4.5) into the above formula, we have

$$\tanh^2 h_3 = \frac{\cosh^2 r (2 \cosh r_1 \cosh r_2 \cosh l_3 - \cosh^2 r_1 - \cosh^2 r_2) - \sinh^2 l_3}{\cosh^2 r (2 \cosh r_1 \cosh r_2 \cosh l_3 - \cosh^2 r_1 - \cosh^2 r_2)}.$$

After substituting the equation $\cosh^2 r = \frac{\mathcal{N}}{\mathcal{D}}$, we have

$$\tanh^2 h_3 = \frac{\mathcal{N}(2 \cosh r_1 \cosh r_2 \cosh l_3 - \cosh^2 r_1 - \cosh^2 r_2) - \mathcal{D} \sinh^2 l_3}{\mathcal{N}(2 \cosh r_1 \cosh r_2 \cosh l_3 - \cosh^2 r_1 - \cosh^2 r_2)}.$$

After substituting the expressions of $\mathcal{N}$ and $\mathcal{D}$ in step 1, we have

$$\tanh^2 h_3 =$$
$$\frac{[(\cosh l_1 \cosh l_3 - \cosh l_2) \cosh r_1 + (\cosh l_2 \cosh l_3 - \cosh l_1) \cosh r_2 - \sinh^2 l_3 \cosh r_3]^2}{\mathcal{N}(2 \cosh r_1 \cosh r_2 \cosh l_3 - \cosh^2 r_1 - \cosh^2 r_2)}.$$

Step 3. *By direct calculation, we have*

$$\frac{\partial \theta_1}{\partial u_2} = \frac{\partial \theta_2}{\partial u_1} = \frac{-1}{\sin \theta_i \sinh l_j \sinh l_k}$$

$$\left(\cosh r_3 - \frac{\cosh l_1 \cosh l_3 - \cosh l_2}{\sinh^2 l_3} \cosh r_1 - \frac{\cosh l_2 \cosh l_3 - \cosh l_1}{\sinh^2 l_3} \cosh r_2 \right) =$$

$$\frac{(\cosh l_1 \cosh l_3 - \cosh l_2) \cosh r_1 + (\cosh l_2 \cosh l_3 - \cosh l_1) \cosh r_2 - \sinh^2 l_3 \cosh r_3}{\sqrt{\mathcal{N}} \cdot \sinh^2 l_3}.$$

Comparing with the last formula of step 2, we have

$$\frac{\partial \theta_1}{\partial u_2} = \frac{\partial \theta_2}{\partial u_1} = \frac{\tanh h_3}{\sinh^2 l_3} \sqrt{2 \cosh r_1 \cosh r_2 \cosh l_3 - \cosh^2 r_1 - \cosh^2 r_2}.$$

4.3. Spherical Case

According to a general principle of the relation of hyperbolic geometry and spherical geometry, to obtain a formula in spherical geometry, we only need to replace $\sinh$ and $\cosh$ in hyperbolic geometry by $\sqrt{-1} \sin$ and $\cos$.

For the mixed type of discrete conformal geometry with spherical background geometry, the edge length of $\triangle_{123}$ is given by

$$\cosh l_{ij} =$$

$$-4\eta_{ij}\frac{\sin r_i}{(1-\varepsilon_i)\cos r_i + 1 + \varepsilon_i}\frac{\sin r_j}{(1-\varepsilon_j)\cos r_j + 1 + \varepsilon_j} + \cos^{\varepsilon_i} r_i \cos^{\varepsilon_j} r_j.$$

Via the cosine law, the edge lengths l_1, l_2, l_3 determine the angles $\theta_1, \theta_2, \theta_3$.

We can define power circles similarly. Let h_i be the distance from the center of the power circle to the edge ij whose length is l_k.

Theorem 4.3. *Let*

$$e^{u_i} = \tan\frac{r_i}{2}.$$

Then

$$\frac{\partial\theta_1}{\partial u_2} = \frac{\partial\theta_2}{\partial u_1}$$

which equal to

$$\frac{\tan h_3}{\sin^2 l_3}\sqrt{-2\cos^{\varepsilon_1} r_1 \cos^{\varepsilon_2} r_2 \cos l_3 + \cos^{2\varepsilon_1} r_1 + \cos^{2\varepsilon_2} r_2}.$$

This gives a geometric proof for the symmetry lemma 3.13 in spherical case.

This theorem is also proved by using the general principle: replace sinh and cosh in hyperbolic geometry by $\sqrt{-1}\sin$ and $\cos$.

Here we can give the second proof for the symmetry lemma 3.13 based on the geometric interpretation to the Hessian, which is geometric and intuitive.

Proof 4.4. *Formula 4.1 show the symmetry for all schemes with Euclidean background geometry; theorem 4.1 proves the symmetry for the hyperbolic cases; theorem 4.3 for the spherical cases.*

5. Geometric Interpretations to Ricci Energies

The geometric interpretation to Ricci energies of Euclidean and hyperbolic Yamabe schemes were discovered by Bobenko, Pinkall and Springborn in [11]. The interpretation to Ricci energies of Euclidean schemes (without the mixed type) are illustrated in [5]. In the current work, we generalize the geometric interpretations to all the schemes in all background geometries covered by the unified framework, as shown in Fig. 13.

We use the upper half space model for $\mathbb{H}^3$, with Riemannian metric
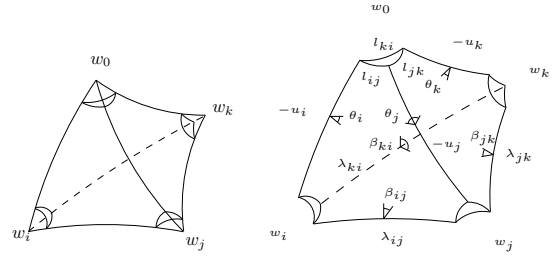
$$ds^2 = \frac{dx^2 + dy^2 + dz^2}{z^2}$$

Figure 9: Generalized hyperbolic tetrahedron.

the xy-plane is the ideal boundary. Consider a triangle $[v_i, v_j, v_k]$, its Ricci energy is closely related to the volume of a generalized hyperbolic tetrahedron whose vertices can be in $\mathbb{H}^3$, truncated by a horosphere or truncated by a hyperbolic plane.

In Fig. 9, the generalized hyperbolic tetrahedron has 4 vertices w_0, w_i, w_j, w_k. The tetrahedron vertex w_0 is called the *top vertex*. The 4 faces of the tetrahedron are hyperbolic planes, the 6 edges are geodesics. The 6 edge lengths of the generalized tetrahedron are $-u_i, -u_j, -u_k$ and $\lambda_{ij}, \lambda_{jk}, \lambda_{ki}$. The generalized tetrahedron is uniquely determined by these 6 edge lengths.

The followings are the common principles for constructing the generalized tetrahedron for all the schemes,

1. For all $\mathbb{E}^2$ schemes, the top vertex w_0 is ideal (at infinity) and truncated by a horosphere; for all $\mathbb{H}^2$ schemes, the top vertex is hyperideal (exceeding the boundary of $\mathbb{H}^3$) and truncated by a hyperbolic plane; for all $\mathbb{S}^2$ schemes, the top vertex is in $\mathbb{H}^3$.

2. For w_i, if the corresponding vertex v_i is of inversive distance circle packing $\varepsilon_i = +1$, then it is hyperideal and truncated by a hyperbolic plane; if v_i is of Yamabe flow $\varepsilon_i = 0$, then it is ideal and truncated by a horosphere; if v_i is virtual radius circle packing $\varepsilon_1 = -1$, then it is in $\mathbb{H}^3$. Same results holds for w_j and w_k.

3. The edges on the truncated tetrahedron, connecting to the top vertex on the original tetrahedron, have lengths $-u_i, -u_j$ and $-u_k$ respectively.

4. For the edge lengths λ_{ij}, there is a unified formula for three geometries: Euclidean, hyperbolic, spherical,

$$\eta_{ij} = \frac{1}{2}(e^{\lambda_{ij}} + \varepsilon_i\varepsilon_j e^{-\lambda_{ij}}). \tag{5.1}$$

The triangle associated to the top vertex w_0 is the triangle $[v_i, v_j, v_k]$. It is obtained by truncating by a horosphere, truncating by a hyperbolic plane or intersecting with a sphere. Given $-u_i, -u_j, -u_k, \eta_{ij}, \eta_{jk}, \eta_{ki}$, using cosine law, we can calculate the edge lengths of the triangle $[v_i, v_j, v_k]$. They are exactly given by the formula Eqn. 3.3. That means the triangle $[v_i, v_j, v_k]$ has lengths l_{ij}, l_{jk}, l_{ki} and angles $\theta_i, \theta_j, \theta_k$.

9

Here we can give the third proof for the symmetry lemma based on the geometric interpretation to the Ricci energy, which is more geometric, intuitive and much easier to verify.

Proof 5.1. *As shown in Fig. 9, for a generalized hyperbolic tetrahedron, the 4 vertices can have any types. The 3 vertical edges have lengths* $-u_i, -u_j, -u_k$ *with dihedral angles* $\theta_i, \theta_j, \theta_k$. *The bottom edges have lengths* $\lambda_{ij}, \lambda_{jk}, \lambda_{ki}$ *with dihedral angles* $\beta_{ij}, \beta_{jk}, \beta_{ki}$.

Let V *be the volume of the generalized hyperbolic tetrahedron. By Schläfli formula*

$$dV = -\frac{1}{2}\left(-u_i d\theta_i - u_j d\theta_j - u_k d\theta_k + \lambda_{ij} d\beta_{ij} + \lambda_{jk} d\beta_{jk} + \lambda_{ki} d\beta_{ki}\right)$$
(5.2)

During the Ricci flow, the conformal structure coefficients $\eta_{ij}, \eta_{jk}, \eta_{ki}$ *are invariant, so* $\lambda_{ij}, \lambda_{jk}, \lambda_{ki}$ *are fixed. Because the generalized tetrahedron is determined by the edge lengths* $-u_i, -u_j, -u_k, \lambda_{ij}, \lambda_{jk}, \lambda_{ki}$, *during the flow, all dihedral angles* $\theta_i, \theta_j, \theta_k, \beta_{ij}, \beta_{jk}, \beta_{ki}$ *are functions of* u_i, u_j, u_k, *the volume* V *is also the function of* u_i, u_j, u_k.

Consider the function,

$$W(u_i, u_j, u_k) = u_i\theta_i + u_j\theta_j + u_k\theta_k - \lambda_{ij}\beta_{ij} - \lambda_{jk}\beta_{jk} - \lambda_{ki}\beta_{ki} - 2V$$
(5.3)

hence,

$$
\begin{aligned}
dW =\ & \theta_i du_i + \theta_j du_j + \theta_k du_k \\
& + u_i d\theta_i + u_j d\theta_j + u_k d\theta_k - \lambda_{ij} d\beta_{ij} - \lambda_{jk} d\beta_{jk} - \lambda_{ki} d\theta_{ki} \\
& - 2dV
\end{aligned}
$$

substitute Schläfli formula Eqn. 5.2, we have

$$dW = \theta_i du_i + \theta_j du_j + \theta_k du_k$$

therefore

$$W = \int \theta_i du_i + \theta_j du_j + \theta_k du_k + c.$$

W *in fact, is the discrete Ricci energy on face in Eqn. 3.5. This shows the differential 1-form*

$$\theta_i du_i + \theta_j du_j + \theta_k du_k \tag{5.4}$$

is exact, therefore closed. Namely, the Hessian matrix

$$\frac{\partial(\theta_i, \theta_j, \theta_k)}{\partial(u_i, u_j, u_k)}$$

is symmetric.

The formula Eqn. 5.3 represents the Ricci energy on a face as the volume of the generalized hyperbolic tetrahedron with other terms of conformal factors and conformal structure coefficients. This formula was introduced first by Bobenko, Pinkall and Springborn in [11] for Euclidean and hyperbolic Yamabe flow. In the current work, we generalize it to all 18 schemes. The differential in Eqn. 5.4 is independent of the choice of horospheres, since the Schläfli formula is independent of the choice of horospher for an ideal vertex.

6. Experimental Results

In this section, we report our experimental results based on unified Ricci flow. We thoroughly compare different schemes in terms of robustness, conformality, efficiency and initialization difficulty.

6.1. Experimental Environment

We implemented the unified Ricci flow algorithms using generic C++ language on Windows platform. The method is based on optimizing the convex energy using Newton's method. The sparse linear systems are solved using Eigen library [45]. The mesh representation is based on dynamic halfedge data structure. The current implementation covers all schemes: tangential circle packing, Thurston's circle packing, inversive distance circle packing, Yamabe flow, virtual radius circle packing and mixed type schemes, for discrete surfaces with Euclidean and hyperbolic background geometries. The algorithms can handle surfaces different topologies. The package is accessible for the whole research community.

The computational time is tested on the desktop with 2.00GHz CPU, 3.00G RAM. The geometric data sets are from the public databases, such as [46] and [47]. The human face surfaces were scanned from a high speed and high resolution, phase shifting scanner, as described in [48]. We tested our algorithm on a huge amount of various models, including different sizes and topology types. Some of them are without any refinement or geometric processing, in order to test the robustness of the algorithms. Some of them are re-meshed using the algorithm in [49].

6.2. Generality Testing

Fig. 1 and 2 demonstrate the generality of Ricci flow method to handle surfaces with all possible topologies. Fig. 1 shows the uniformization for closed surfaces, where surfaces are conformally mapped to the unit sphere, Euclidean plane or the hyperbolic disk. Fig. 2 illustrates the uniformization for surfaces with boundaries, where compact surface with boundaries are mapped to constant curvature spaces, such that all boundaries are mapped to geodesic circles. Suggested by Glickenstein: Although there is not currently a robust theory of Ricci flow with boundary in the smooth setting, the discrete Ricci flow can compute the canonical conformal mapping with high efficacy and efficiency. These two figures cover all the topology types of compact surfaces.

10

(a) low quality face　　(b) high quality face

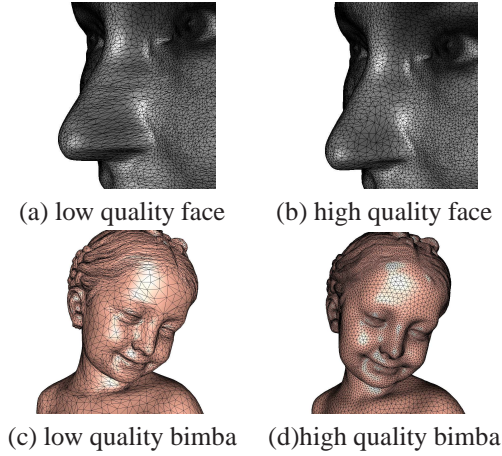(c) low quality bimba　　(d)high quality bimba

Figure 10: Robustness testing.

The uniformization of the genus zero closed surface can be computed using Ricci flow with spherical background geometry, or Euclidean background geometry. The spherical Ricci energy is non-convex, therefore the spherical Ricci flow is not so stable as the Euclidean Ricci flow. For surface with multiple boundaries, we used Ricci flow method with Koebe's iteration [50].

6.3. Comparisons Among Schemes

In the following we compare different schemes of surface Ricci flow in details.

Robustness. In practice, the biggest challenge for Ricci flow algorithm is the robustness. Given a target curvature $\bar{K}$, we need to ensure the following two points:

1. The target curvature is admissible, namely, the solution to the Ricci flow Eqn. 3.4 exists.
2. The solution is reachable. It is possible that the flow hits the boundary of the admissible curvature space before it hits the target curvature.

For Tangential circle packing, Thurston's circle packing, there are theorems describing the admissible curvature spaces [13] and [9]. For Euclidean (or hyperbolic) Yamabe flow, if the Delaunay condition is preserved during the flow by edge swapping, the admissible curvature space is given in the recent works [29] and [30].

We test robustness to the mesh qualities of different schemes. As shown in Fig. 10, the low quality meshes are simplified from the raw data, they have many obtuse angles and degenerated triangles; the high quality meshes are obtained using the method in [49]. We use different schemes to compute Riemann mappings. For surfaces with high mesh qualities, all schemes succeed with comparable running time. For surfaces with low

mesh qualities, tangential circle packing outperforms all other schemes. The other schemes either crash in the flow process, or pass through with carefully chosen small step length, therefore, the running times are much longer.

If we allow the connectivity to be modified during the flow, to preserve the power Delaunay condition, then all schemes succeed on both surfaces. This shows the preserving the power Delaunay condition greatly improves the robustness of the Ricci flow algorithms.

Conformality. Fig. 11 compares the qualities of different schemes: tangential circle packing, inversive distance circle packing, Yamabe flow and virtual radius circle packing. The parameterization is denoted as $\varphi : M \to \mathbb{R}^2$. We calculate each corner angle in the mesh before and after the discrete conformal mapping. Then we compute the ratio between two angle values, take the logarithm. The histogram of the logarithm of the angle ratios is a good measurement for the quality of the discrete conformal mapping. If the mapping has high conformality, then all angle ratios are close to 1, and the histogram is a delta function at 0. Otherwise, the histogram is with high standard deviation. From the histograms in Fig. 11, we can see the tangential circle packing produces mappings with lower conformity. The other three schemes produce mappings with similar conformality.

Convergence Rate. Fig. 12 and table 1 show one experiment for comparing the convergence rates of different schemes on four different genus one surfaces. In the experiment, the curvature error threshold is set to $1e-6$ the step length in Newton's method is chosen to be $5e-1$. In the table 1, each item shows the running time in seconds, and iterations in the optimization. From the table, we can see the running time and iterations of different schemes are similar.

In practice, tangential circle packing is more robust to lower quality mesh qualities, the step length can be chosen to be larger, therefore, it converges faster than other schemes.

Initialization. In practice, the discrete surfaces are given as triangular meshes, in the initialization stage, we need to convert the edge length function to circle packing metric $(\Sigma, \gamma, \eta, \varepsilon)$. For different schemes, this conversion has different level of difficulties.

For tangential circle packing and Yamabe flow, the initializations are easy and the resulting circle packing metrics are unique. The initialization is difficult for Thurston's circle packing, which requires the intersection angles between two vertex circles are acute, furthermore, the resulting conformal structure coefficient

Tangential CP

Inversive distance CP

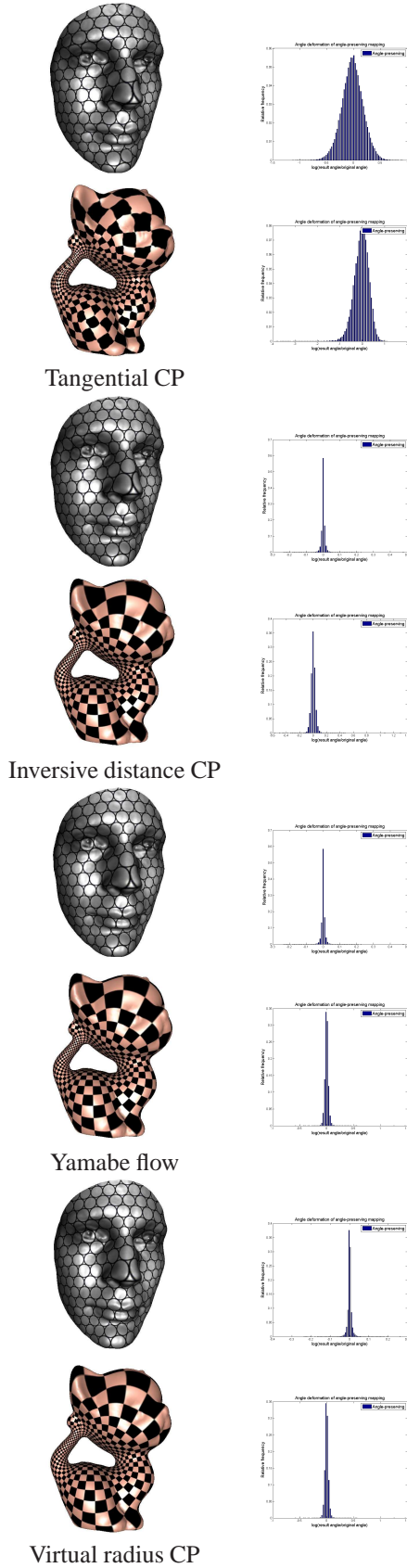Yamabe flow

Virtual radius CP

Figure 11: Conformality test for different schemes. The face model is with high mesh quality, the kitten model is with lower mesh quality.
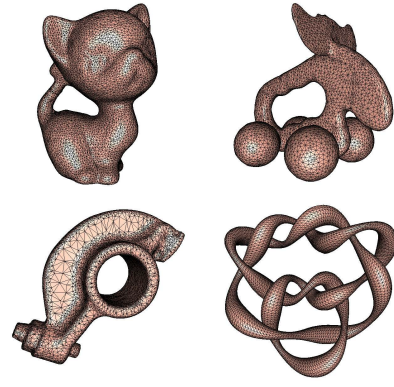

Figure 12: Convergence testing.

mesh	V/F/E	Tan. CP	Inv. Dist. CP	Yamabe Flow	Vir. Rad. CP
Knot	9792/19584/29376	2.324/18	2.314/17	2.223/17	2.234/17
Elk	9000/18000/27000	3.476/24	2.775/28	2.938/21	2.737/20
Rocker	10044/20088/30132	3.424/23	2.891/21	2.938/21	2.922/21
Kitten	10219/20438/30657	4.298/23	3.941/21	3.933/21	3.896/21

Table 1: Convergence test.

$\eta : E \to \mathbb{R}$ may not be unique. For inversive distance, virtual radius and mixed type schemes, the initializations are relatively easier, but the resulting circle packing metrics may not be unique.

In theory, the conformal structure coefficient η will affect the admissible curvature space [13] and [9]. In practice, we haven't found that different choices of η's make differences in terms of conformality or robustness.

7. Conclusion

This work establishes a unified framework for discrete surface Ricci flow, which covers most existing schemes: tangential circle packing, Thurston's circle packing, inversive distance circle packing, discrete Yamabe flow, virtual radius circle packing and mixed scheme, with Spherical, Euclidean and hyperbolic background geometry. The unified frameworks for hyperbolic and spherical schemes are introduced to the literature for the first time. For Euclidean schemes, our formulation is equivalent to Glickenstein's geometric construction.

Four newly discovered schemes are introduced, which are hyperbolic and Euclidean virtual radius circle packing and the mixed schemes.

This work introduces a geometric interpretation to the Hessian of discrete Ricci energy for all schemes, which generalizes Glickenstein's formulation in Euclidean case.

This work also gives explicit geometric interpretations to the discrete Ricci energy for all the schemes, which generalizes Bobenko, Pinkall and Springborn's construction [11] for Yamabe flow cases.

The unified frame work deepen our understanding to the the discrete surface Ricci flow theory, and inspired

12

us to discover the novel schemes of virtual radius circle packing and the mixed scheme, improved the flexibility and robustness of the algorithms, greatly simplified the implementation and improved the efficiency.

Experimental results show the unified surface Ricci flow algorithms can handle surfaces with all possible topologies. We further compare different schemes in terms of conformality, robustness, convergence rate, and the difficulty level of construction.

In the future, we will focus on answering the following open problems: whether all possible discrete surface Ricci flow schemes are the variations of the current unified approach on the primal meshes and the dual diagrams and so on.

References

[1] M. Jin, J. Kim, F. Luo, X. Gu, Discrete surface Ricci flow, IEEE Transactions on Visualization and Computer Graphics 14 (2008) 1030–1043.

[2] W. Zeng, D. Samaras, X. D. Gu, Ricci flow for 3D shape analysis, IEEE Transactions on Pattern Analysis and Machine Intelligence 32 (2010) 662–677.

[3] X. Gu, Y. He, M. Jin, F. Luo, H. Qin, S.-T. Yau, Manifold splines with a single extraordinary point, Computer-Aided Design 40 (2008) 676–690.

[4] W. Zeng, J. Marino, K. Gurijala, X. Gu, A. Kaufman, Supine and prone colon registration using quasi-conformal mapping, IEEE Transactions on Visualization and Computer Graphics) 16 (2010) 1348–1357.

[5] W. Zeng, X. Gu, Ricci Flow for Shape Analysis and Surface Registration, SpringerBriefs in Mathematics, Springer New York, 2013.

[6] R. Hamilton, Ricci flow on surfaces, Mathematics and General Relativity, Contemporary Mathematics AMS, Providence, RI, 71 (1988) 237–261.

[7] B. Chow, The Ricci flow on the 2-sphere, Journal of Differential Geometry 33 (1991) 325–334.

[8] B. Rodin, D. Sullivan, The convergence of circle packings to the Riemann mapping, Journal of Differential Geometry 26 (1987) 349–360.

[9] B. Chow, F. Luo, Combinatorial Ricci flows on surfaces, Journal Differential Geometry 63 (2003) 97–129.

[10] D. Glickenstein, Discrete conformal variations and scalar curvature on piecewise flat two and three dimensional manifolds, Journal of Differential Geometry 87 (2011) 201–238.

[11] A. Bobenko, U. Pinkall, B. Springborn, Discrete conformal maps and ideal hyperbolic polyhedra, arXiv:1005.2698, 2010.

[12] D. Glickenstein, J. Thomas, Duality structures and discrete conformal variations of euclidean and hyperbolic triangles, Preprint (2014).

[13] W. P. Thurston, The Geometry and Topology of 3-manifolds, Princeton University Press, 1981.

[14] E. M. Andreev, Complex polyhedra in Lobachevsky spaces, (Russian) Mat. Sb. (N.S.) 81 (1970) 445–478.

[15] E. M. Andreev, Convex polyhedra of finite volume in Lobachevsky space, (Russian) Mat. Sb. (N.S.) 83 (1970) 256–260.

[16] P. Koebe, Kontaktprobleme der konformen abbildung, Ber. Sächs. Akad. Wiss. Leipzig, Math. Phys. Kl. 88 (1936) 141–164.

[17] A. Marden, B. Rodin, Computational methods and function theory (Valpara'iso,1989), volume 1435 of *Lecture Notes in Math.*, Springer, Berlin, 1990, pp. 103–116.

[18] Y. C. de Verdiére, Un principe variationnel pour les empilements de cercles, Invent. Math. 104 (1991) 655–669.

[19] K. Stephenson, Introduction to Circle Packing: The Theory of Discrete Analytic Functions, Cambridge University Press, 2005.

[20] Z.-X. He, O. Schramm, On the convergence of circle packings to the Riemann map, Invent. Math. 125 (1996) 285–305.

[21] P. L. Bowers, K. Stephenson, Uniformizing dessins and Belyi maps via circle packing, Mem. Amer. Math. Soc. 170 (2004).

[22] R. Guo, Local rigidity of inversive distance circle packing, Trans. Amer. Math. Soc. 363 (2011) 4757–4776.

[23] F. Luo, Rigidity of polyhedral surfaces, iii, Geometry and Topology 15 (2011) 2299–2319.

[24] F. Luo, Combinatorial Yamabe flow on surfaces, Contemp. Math. 6 (2004) 765–780.

[25] B. Springborn, P. Schröder, U. Pinkall, Conformal equivalence of triangle meshes, ACM Trans. Graph. 27 (2008) 1–11.

[26] D. Glickenstein, A combinatorial Yamabe flow in three dimensions, Topology 44 (2005) 791–808.

[27] D. Glickenstein, A maximum principle for combinatorial Yamabe flow, Topology 44 (2005) 809–825.

[28] R. Guo, Combinatorial Yamabe flow on hyperbolic surfaces with boundary, Communications in Contemporary Mathematics 13 (2011) 827–842.

[29] X. Gu, F. Luo, J. Sun, T. Wu, A discrete uniformization theorem for polyhedral surfaces, arXiv:1309.4175 (2013).

[30] X. Gu, R. Guo, F. Luo, J. Sun, T. Wu, A discrete uniformization theorem for polyhedral surfaces ii, arXiv:1401.4594 (2014).

[31] D. Glickenstein, Problems in combinatorial and numerical ricci flow, Talk in Workshop: Perspective Of The Ricci Flow, 2013.

[32] W.Brägger, Kreispackungen und triangulierugen, Enseign. Math. 38 (1992) 201–217.

[33] I. Rivin, Euclidean structures of simplicial surfaces and hyperbolic volume, Ann. of Math. 139 (1994) 553–580.

[34] G. Leibon, Characterizing the Delaunay decompositions of compact hyperbolic surface, Geom. Topol. 6 (2002) 361–391.

[35] A. I. Bobenko, B. A. Springborn, Variational principles for circle patterns and Koebe's theorem, Trans. Amer. Math. Soc. 356 (2004) 659–689.

[36] R. Guo, F. Luo, Rigidity of polyhedral surface ii, Geom. Topol. 13 (2009) 1265–1312.

[37] B. Springborn, A variational principle for weighted Delaunay triangulation and hyperideal polyhedra, Journal of Differential Geometry 78 (2008) 333–367.

[38] F. Luo, Rigidity of polyhedral surfaces, Journal of Differential Geometry 96 (2014) 241–302.

[39] F. Luo, X. Gu, J. Dai, Variational Principles for Discrete Surfaces, Advanced Lectures in Mathematics, High Education Press and International Press, 2007.

[40] S. Hersonsky, Boundary value problems on planar graphs and flat surfaces with integer cone singularities, i: The dirichlet problem, J. Reine Angew. Math. (2012) 65–92.

[41] S. Hersonsky, The triple intersection property, three dimensional extremal length, and tiling of a topological cube, Topology Appl. 159 (2012) 2795–2805.

[42] S. Hersonsky, Boundary value problems on planar graphs and flat surfaces with integer cone singularities, ii: the mixed dirichlet-neumann problem, Differential Geom. Appl. 29 (2011) 329–347.

[43] S. Hersonsky, Energy and length in a topological planar quadrilateral, European J. Combin. 29 (2011) 208–217.

[44] Z-X.He, Rigidity of infinite disk patterns, Ann. of Math 149 (1999) 1–33.

[45] G. Guennebaud, B. Jacob, et al., Eigen, http://eigen.tuxfamily.org, 2010.

[46] The digital michelangelo project, https://graphics.stanford.edu/projects/mich/, 1997.

[47] Repository of aim@shape project, http://shapes.aimatshape.net/, 1997.

[48] Y. Wang, M. Gupta, S. Zhang, S. Wang, X. Gu, D. Samaras, P. Huang, High resolution tracking of non-rigid motion of densely sampled 3d data using harmonic maps, International Journal of Computer Vision 76 (2008) 283–300.

[49] H.Li, W.Zeng, J-M.Morvan, L.Chen, X.Gu, Surface meshing with curvature convergence, IEEE Transactions on Visualization and Computer Graphics 99 (2013) 1.

[50] M.Zhang, Y. Li, W. Zeng, X. Gu, Canonical conformal mapping for high genus surfaces with boundaries, Computers and Graphics 36 (2012) 417–426.

Appendix

In the appendix, we explain the unified surface Ricci flow algorithm 1 in details, and reorganize all the formulae necessary for the coding purpose.

Algorithm 1 Unified Surface Ricci Flow

Require: The inputs include:
    1. A triangular mesh Σ, embedded in $\mathbb{E}^3$;
    2. The background geometry, $\mathbb{E}^2$, $\mathbb{H}^2$ or $\mathbb{S}^2$;
    3. The circle packing scheme, $\varepsilon \in \{+1, 0, -1\}$;
    4. A target curvature $\bar{K}$, $\sum \bar{K}_i = 2\pi\chi(\Sigma)$ and $\bar{K}_i \in (-\infty, 2\pi)$.
    5. Step length δt
Ensure: A discrete metric conformal to the original one, which realizes the target curvature $\bar{K}$.
  1: Initialize the circle radii γ, discrete conformal factor u and conformal structure coefficient η, obtain the initial circle packing metric $(\Sigma, \gamma, \eta, \varepsilon)$
  2: **while** $\max_i |\bar{K}_i - K_i| > threshold$ **do**
  3:     Compute the circle radii γ from the conformal factor u
  4:     Compute the edge length from γ and η
  5:     Compute the corner angle θ_i^{jk} from the edge length using cosine law
  6:     Compute the vertex curvature K
  7:     Compute the Hessian matrix H
  8:     Solve linear system $H\delta u = \bar{K} - K$
  9:     Update conformal factor $u \leftarrow u - \delta t \times \delta u$
 10: **end while**
 11: Output the result circle packing metric.

Step 1. Initial Circle Packing (γ, η). Depending on different schemes, the initialization of the circle packing is different. The mesh has induced Euclidean metric l_{ij}. For inversive distance circle packing, we choose

$$\gamma_i = \frac{1}{3} \min_j l_{ij},$$

this ensures all the vertex circles are separated. For Yamabe flow, we choose all γ_i to be 1. For virtual radius circle packing, we choose all γ_i's to be 1. Then γ_{ij} can be computed using the l_{ij} formula in Tab. 2.

Step 3. Circle Radii γ. The computation for circle radii from conformal factor uses the formulae in the first column in Tab.2.

	u_i	Edge Length l_{ij}	$\tau(i,j,k)$	$s(x)$
$\mathbb{E}^2$	$\log \gamma_i$	$l_{ij}^2 = 2\eta_{ij}e^{u_i+u_j} + \varepsilon_i e^{2u_i} + \varepsilon_j e^{2u_j}$	$\frac{1}{2}(l_i^2 + \varepsilon_j\gamma_j^2 - \varepsilon_k\gamma_k^2)$	x
$\mathbb{H}^2$	$\log\tanh\frac{\gamma_i}{2}$	$\cosh l_{ij} = \frac{4\eta_{ij} + (1+\varepsilon_i e^{2u_i})(1+\varepsilon_j e^{2u_j})}{(1-\varepsilon_i e^{2u_i})(1-\varepsilon_j e^{2u_j})}$	$\cosh l_i \cosh^{\varepsilon_j}\gamma_j - \cosh^{\varepsilon_k}\gamma_k$	$\sinh x$
$\mathbb{S}^2$	$\log\tan\frac{\gamma_i}{2}$	$\cos l_{ij} = \frac{4\eta_{ij} + (1-\varepsilon_i e^{2u_i})(1-\varepsilon_j e^{2u_j})}{(1+\varepsilon_i e^{2u_i})(1+\varepsilon_j e^{2u_j})}$	$\cos l_i \cos^{\varepsilon_j}\gamma_j - \cos^{\varepsilon_k}\gamma_k$	$\sin x$

Table 2: Formulae for $\mathbb{E}^2$, $\mathbb{H}^2$ and $\mathbb{S}^2$ background geometries.

Step 4. Edge Length l. The computation of edge lengths from conformal factor u and conformal structure coefficient η uses the formulae in the 2nd column in Tab.2

Step 5. Corner Angle θ. The computation from edge length l to the corner angle θ uses the cosine law formulae,

$$
\begin{aligned}
l_k^2 &= \gamma_i^2 + \gamma_j^2 - 2l_i l_j \cos\theta_k & \mathbb{E}^2 \\
\cosh l_k &= \cosh l_i \cosh l_j - \sinh l_i \sinh l_j \cos\theta_k & \mathbb{H}^2 \\
\cos l_k &= \cos l_i \cos l_j - \sin l_i \sin l_j \cos\theta_k & \mathbb{S}^2
\end{aligned}
$$

Step 6. Vertex Curvature K. The vertex curvature is defined as angle deficit

$$
K(v_i) = \begin{cases} 2\pi - \sum_{[v_i,v_j,v_k]} \theta_i^{jk} & v_i \notin \partial\Sigma \\ \pi - \sum_{[v_i,v_j,v_k]} \theta_i^{jk} & v_i \notin \partial\Sigma \end{cases}
$$

Step 7. Hessian Matrix H.

$$\frac{\partial(\theta_i, \theta_j, \theta_k)}{\partial(u_i, u_j, u_k)} = -\frac{1}{2A}L\Theta L^{-1}D,$$

where

$$A = \sin\theta_i s(l_j)s(l_k),$$

and

$$L = diag(s(l_i), s(l_j), s(l_k)),$$

and

$$
D = \begin{pmatrix} 0 & \tau(i,j,k) & \tau(i,k,j) \\ \tau(j,i,k) & 0 & \tau(j,k,i) \\ \tau(k,i,j) & \tau(k,j,i) & 0 \end{pmatrix}.
$$

Step. 8 Linear System. If the Σ is with $\mathbb{H}^2$ background geometry, then the Hessian matrix H is positive define; else if Σ is with $\mathbb{E}^2$ background geometry, then H is positive definite on the linear subspace $\sum_i u_i = 0$. The linear system can be solved using any sparse linear solver, such as Eigen [45].

For discrete surface Ricci flow with topological surgeries, we can add one more step right after step 4. In this new step, we modify the connectivity of Σ to keep the triangulation to be (Power) Delaunay. This will greatly improves the robustness as proved in [29] and [30].
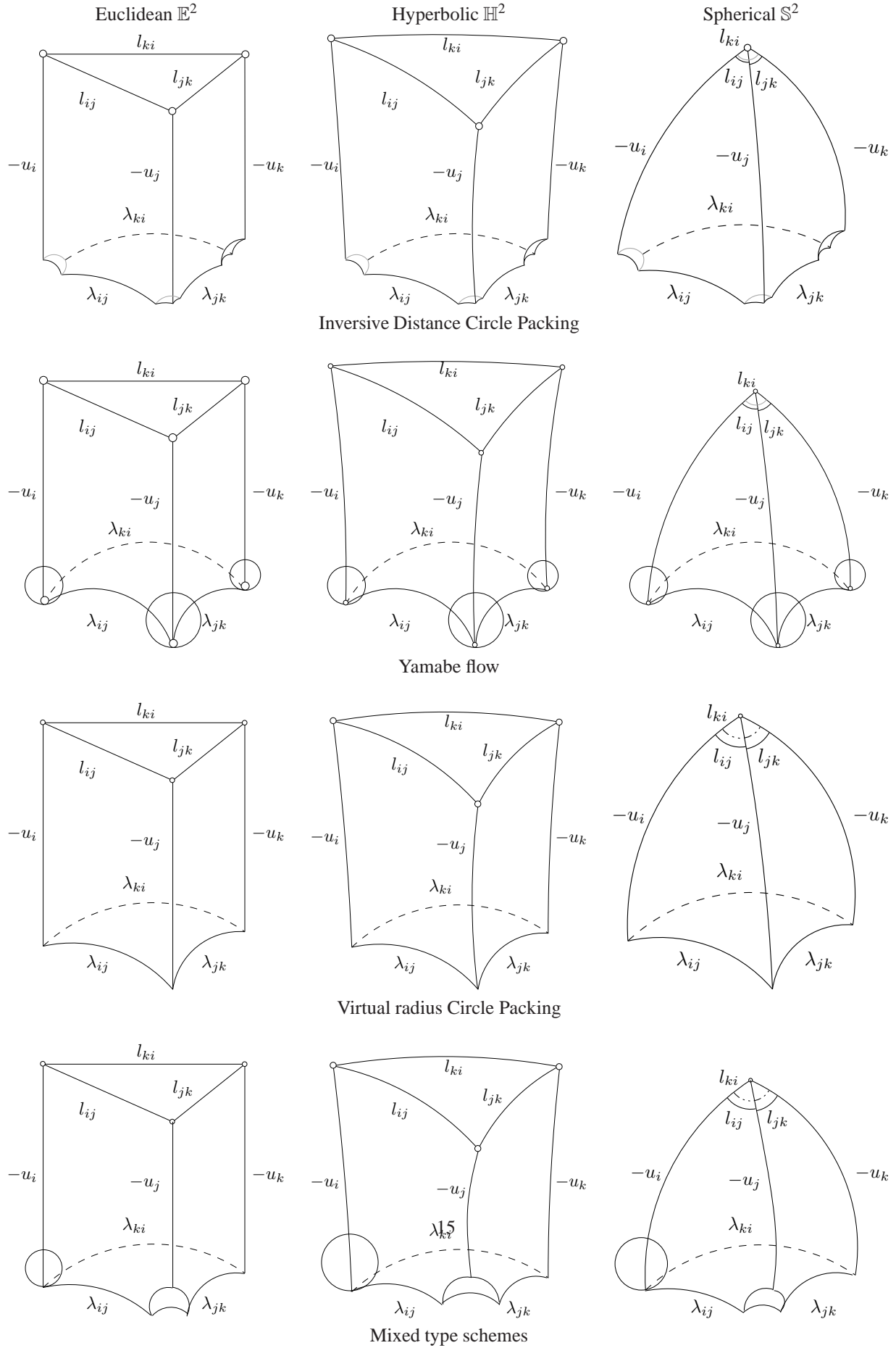
14

Figure 13: Geometric interpretation to discrete Ricci energy - volumes of generalized hyperbolic tetrahedra.